ChemComm

Check for updates

A biomarker-responsive nanoprobe for detecting hepatic ischemia-reperfusion injury *via* optoacoustic/NIR-II fluorescence imaging†

Zhuo Zeng, Junjie Chen, Lihe Sun, Fang Zeng (ID) * and Shuizhu Wu (ID) *

A nanoprobe for detecting hepatic ischemia-reperfusion injury has been developed. Apparent optoacoustic and NIR-II fluorescent signals are given out upon the nanoprobe's response to the *in situ* biomarker H_2O_2 in the liver in the case of ischemia-reperfusion injury.

Hepatic ischemia-reperfusion injury (HIRI) is a primary cause of liver damage and a common major complication in liver surgeries including liver transplantation/engraftment and hepatic resection.[1,2] HIRI is typified by an inflammatory response and is the key cause for early or late liver dysfunction resulting in a high incidence of chronic or acute rejection as well as ultimate failure after liver transplantation, which further exacerbates the acute shortage of livers available for life-saving transplantation.[2,3] HIRI is a multifactorial and complex pathophysiological process that is often involved in adverse clinical outcomes.[4] Excessive production of reactive oxygen species (ROS) has been recognized as the critical factor in the genesis of HIRI and the crucial pathophysiological mechanism in HIRI.[4,5] ROS, in particular H_2O_2 as the most stable and abundant ROS member, overproduced during reperfusion would directly cause tissue damage and set in motion a cascade of harmful reactions that lead to inflammation, cell death or even organ failure.[4–6] Consequently, hepatic H_2O_2 can be employed as the *in situ* endogenous biomarker for HIRI. Once HIRI can be identified in the early phase, effective preventative or therapeutic strategies can be adopted to minimize the injury induced by ischemia and reperfusion processes during and/or after liver operations. Therefore, effective non-invasive detection/diagnostic approaches are essential for the avoidance of HIRI and thus saving lives.

Fluorescence noninvasive imaging in the second near-infrared (NIR-II, 900–1700 nm) window can facilitate imaging

State Key Laboratory of Luminescent Materials and Devices, Guangdong Provincial Key Laboratory of Luminescence from Molecular Aggregates, College of Materials Science and Engineering, South China University of Technology, Guangzhou 510640, China. E-mail: mcfzeng@scut.edu.cn, shzhwu@scut.edu.cn

† Electronic supplementary information (ESI) available: Experimental procedures, the probe's synthetic route, NMR/mass spectra, absorption/fluorescence spectra, cell viabilities, H&E staining images, NIR-II fluorescence images and MSOT images. See DOI: https://doi.org/10.1039/d2cc06031k

with greater penetration depth and enhanced sensitivity owing to the reduced photon scattering and low auto-fluorescence of tissues in this wavelength range.[7–11] Meanwhile, optoacoustic imaging is a non-invasive hybrid imaging modality, which combines the advantages of optical imaging and ultrasound imaging while avoiding the limitations of pure optical imaging.[12–14] Among optoacoustic imaging methods, multispectral optoacoustic tomography imaging (also known as MSOT imaging) is a functional optoacoustic imaging method; owing to the excitation by multiwavelength laser pulses and the probe-specific spectral unmixing, the reconstructed MSOT images can depict the spatiotemporal distribution of the specific probe or contrast agent in biological samples based on the spectral identification of the probe or contrast agent; consequently, the 3D MSOT images (*e.g.*, orthogonal-view 3D images) would facilitate the accurate determination of the precise locality and size of the lesion or infection.[15–20] Aided by biomarker-responsive probes, the integration of NIR-II fluorescence imaging and MSOT imaging would constitute an effective means for high-quality bioimaging which ensures that the obtained results are corroboratory.

Boron-dipyrromethene (BODIPY) dyes possess high quantum yield and easy structural modification,[21] but the large planar conjugation of BODIPY-based NIR-II dyes causes such primary limitations as low water solubility/dispersibility, which hamper their biological applications in aqueous milieu. Hence, a water soluble or dispersible biomarker-responsive probe based on NIR-II BODIPY-type dyes together with NIR-II fluorescence imaging and MSOT imaging would synchronously offer biomarker-activatable detection and accurate delineation of the disease sites. In view of the above considerations, herein we designed a biomarker (H_2O_2)-responsive nanoprobe BX-BOH@BSA for the detection and imaging of HIRI *via* NIR-II fluorescence and MSOT imaging. The biofriendly and hydrophilic albumin (bovine serum albumin: BSA) serves as the matrix for encapsulating the molecular probe BX-BOH to form the nanoprobe BX-BOH@BSA, which ensures sufficient water dispersibility and good biocompatibility for biological applications. The fluorescence of the nanoprobe itself (BX-BOH@BSA) is rather weak; whereas the presence of H_2O_2 leads to the evident enhancement of the fluorescent and

Scheme 1 Illustrative scheme for the nanoprobe BX-BOH@BSA's formation and its detection of HIRI *via* responding to H_2O_2 in a mouse model with optoacoustic and NIR-II fluorescence imaging.

Fig. 1 (A) NIR-II fluorescence spectra for BX-BOH@BSA (0.6 mg mL^{-1}) without and with incubation with H_2O_2 in PBS (with 5% DMSO, pH 7.4). (B) Fluorescence intensity at 938 nm for BX-BOH@BSA (0.6 mg mL^{-1}) without or with incubation with H_2O_2 in PBS (with 5% DMSO, pH 7.4) ($n = 3$). (C) NIR-II fluorescence spectra of BX-BOH, BX-BOH@BSA and BX-BOH@BSA + H_2O_2 upon reaction with H_2O_2 (90 μM), respectively. (D) HPLC chromatograms for BX-BOH, BX, and BX-BOH were treated with H_2O_2 for 40 min (MeOH is the mobile phase with 1.0 mL min^{-1} flow rate).

optoacoustic signals due to the removal of the methylphenyl boronate group and the subsequent transformation of quaternized pyridyl into the uncharged pyridyl group (Scheme 1). The nanoprobe has been utilized in detecting and imaging HIRI in a mouse model through responding to the biomarker H_2O_2 in the hepatic region.

The molecular probe BX-BOH was prepared according to the synthesis process in Scheme S1 (ESI†). And the related characterization data (NMR and HRMS spectra) are presented in Fig. S1–S6 (ESI†). The molecular probe BX-BOH was obtained with 4-(bromomethyl)phenyl boronic acid being incorporated onto the NIR-II dye BX through the *N*-alkylation reaction of the pyridine group, by which the strong electron-pulling group quaternized pyridyl was formed. This quaternized pyridyl group (electron-pulling) plays a fluorescence-quenching role due to the photoinduced electron transfer effect,[22] while the xanthene derivative is the electron-pushing moiety, and the methylphenyl boronate acts as a H_2O_2 responsive group. With BSA as the matrix to encapsulate the molecular probe BX-BOH molecules in PBS, the nanoprobe BX-BOH@BSA was prepared. The particle size distribution of the nanoprobe BX-BOH@BSA and the activated nanoprobe BX@BSA was assessed by the dynamic light scattering method, and from Fig. S7 (ESI†) it is clear that the hydrodynamic size of the BX-BOH@BSA and BX@BSA nanoparticles is about 25 nm and 20 nm.

The nanoprobe BX-BOH@BSA's spectral response toward H_2O_2 was first investigated in PBS (containing 5% DMSO, pH 7.4). As presented in Fig. 1A and B, the H_2O_2-concentration-dependent fluorescence "turn-on" response (900–1300 nm with peak at 938 nm) can be clearly observed. The nanoprobe

BX-BOH@BSA's time-dependent fluorescence spectra exhibit that the response reaches the maximal level in around 80 min (Fig. S8, ESI†). In addition, the nanoprobe BX-BOH@BSA's optoacoustic intensity displays the H_2O_2-concentration-dependent enhancement (Fig. S9, ESI†), as the nanoprobe's absorption in the 650–950 nm range increases significantly upon responding to H_2O_2 (Fig. S10, ESI†). The limit of detection of the nanoprobe for H_2O_2 is determined as 0.77 μM ($3\sigma/k$). The extinction coefficient and fluorescence quantum yield of the nanoprobe after the response is 6.7×10^2 mL g^{-1} cm^{-1} and 0.46% (the reference standard: quantum yield 0.5% of 1,2-dichloroethane). The similarities of the fluorescence and absorption spectra between the probe compound BX-BOH and the nanoprobe BX-BOH@BSA, together with the zeta potentials of BX-OH and BX-BOH@BSA being slightly positive and negative (-27.9 mV), respectively, support that the molecular probe BX-BOH molecules were successfully encapsulated in the BSA matrix (Fig. S10, ESI†). It is indubitable from these spectral data that BX-BOH@BSA can detect H_2O_2 with turn-on optoacoustic and NIR-II fluorescent signals.

To corroborate the molecular probe BX-BOH's response mechanism for H_2O_2, HPLC measurements were performed. As shown in Fig. 1D, the values of the retention time for the chromophore BX and the probe compound BX-BOH are 6.48 and 2.00 min, respectively. After incubation with H_2O_2, the peak of retention time for the probe compound BX-BOH decreases, while the retention time peak corresponding to BX appears, which substantiates that the reaction of the probe compound with H_2O_2 produces the chromophore BX. Afterwards, the response selectivity of the nanoprobe BX-BOH@BSA was tested with some biologically-related substances (Fig. S11, ESI†); it is

clear to be seen that the nanoprobe BX-BOH@BSA's response toward H_2O_2 has relatively good selectivity. Based on density functional theory (DFT) calculation for BX-BOH and BX (Table S1, ESI†), the energy gap supports the slightly blue-shifted change of absorption due to the transformation from BX-BOH to BX induced by H_2O_2.

Before applying the nanoprobe BX-BOH@BSA in animal experiments, we investigated the nanoprobe BX-BOH@BSA's biosafety. In this regard, firstly, we adopted the commonly-used MTT assay; as presented in Fig. S12 (ESI†), BX-BOH@BSA's cytotoxicities toward mouse fibroblast cells (L929 cells) are quite low. Secondly, healthy mice were randomly assigned to two groups (5 mice per group) with one group receiving i.v. injection of the nanoprobe BX-BOH@BSA and the other group receiving saline for 7 days. The mice's body weights were monitored daily for 7 days after the injection (Fig. S13, ESI†). It is clear that no obvious changes or differences exist in the mice's body weights for these 7 days. Furthermore, 7 days after injection of the nanoprobe or saline, the mice's main organs (heart, spleen, liver, kidney and lung) were collected upon the mice being euthanized and the histological analysis was conducted *via* H&E staining (Fig. S14, ESI†). The histological data unambiguously exhibit that no discernible damage to these main organs of the mice exists after 7 days' injection of the nanoprobe BX-BOH@BSA. These results support that the nanoprobe BX-BOH@BSA's biosafety is relatively good, which is appropriate for *in vivo* experimental applications.

Afterwards, the nanoprobe BX-BOH@BSA was applied in a mouse model to detect and monitor HIRI. For this purpose, the HIRI mouse model was established by following the previously-reported method.[23] And the experimental protocol is shown in Fig. S22A (ESI†). In this experiment, four groups of healthy mice were used. Among them, the mice of the first group underwent ischemia for the time period of 30 min, which was followed by 24 h reperfusion (notated as "I/R: 30 min/24 h"). The mice of the second group underwent ischemia for the time period of 60 min, which was followed by 24 h reperfusion (notated as "I/R: 60 min/24 h"). The mice of the third group underwent 0 min ischemia (the sham group, notated as "Sham"). The mice of the fourth group (notated as "NAC") underwent ischemia for the time period of 60 min which was followed by 24 h reperfusion and then were treated with an antioxidative drug *N*-acetylcysteine (NAC) (150 mg kg^{-1} body weight daily starting from 2 d prior to the ischemia procedure) according to the reported treatment method.[24]

Subsequently, the different groups of mice were i.v. injected with BX-BOH@BSA (4.0 mg kg^{-1}) and NIR-II fluorescent imaging was carried out. It is clearly seen from Fig. 2B and C that for the sham group, only rather weak fluorescence exists in the mice's liver region at 90 min after the nanoprobe BX-BOH@BSA's injection; contrarily, for the ischemia groups, the mice's liver region shows much more significantly evident fluorescent signals at the same time points. In addition, for the mice undergoing longer time of ischemia (ischemia for 60 min), stronger fluorescent signals can be observed, owing to more hepatic H_2O_2 generated by longer ischemia time followed by reperfusion. Notably, as for the mice receiving treatment with NAC, there exist much weaker fluorescence signals in
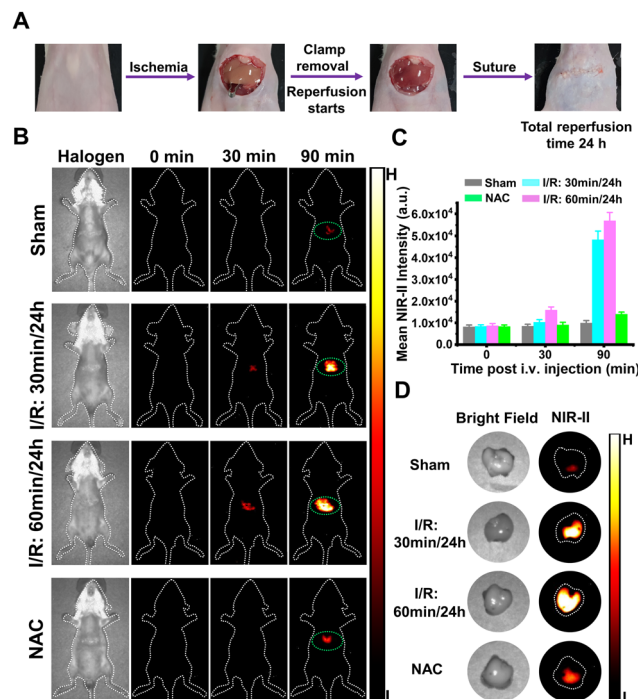

Fig. 2 (A) Illustration of the experimental process for the HIRI mouse model. (B) NIR-II fluorescent images of the sham group (0 min ischemia) and the HIRI model groups (with 30 min or 60 min ischemia followed by 24 h reperfusion) at 0, 30, or 90 min after BX-BOH@BSA's i.v. injection (4.0 mg kg^{-1}). Mice were in supine posture. The liver region is shown by the green dotted line. (C) Average NIR-II fluorescent intensities of the liver region (ROI shown by green dotted line) corresponding to the mice of (B) ($n = 5$). (D) Bright-field images (on the left) and NIR-II fluorescent images (on the right) of the mice's livers at 90 min after BX-BOH@BSA's i.v. injection (4.0 mg kg^{-1}).

comparison to the groups without NAC treatment, because NAC scavenges much H_2O_2. In addition, for all the groups, the livers' *ex vivo* NIR-II fluorescent imaging data clearly show evident fluorescent signals which enhances the lengthening ischemia time (Fig. 2D and Fig. S15, ESI†).

Furthermore, the main organs (such as heart, spleen, liver, kidney and lung) were gathered from all the groups for MSOT imaging (Fig. S21, ESI†). Obviously, the optoacoustic signals exist in the liver, and the mice's liver of the "I/R: 30 min/24 h" group or "I/R: 60 min/24 h" group exhibits much stronger optoacoustic signals compared to other organs.

Furthermore, the nanoprobe BX-BOH@BSA was employed in MSOT imaging for detecting HIRI in the mice. The scanning range for MSOT imaging is shown in Fig. S16 (ESI†). From the orthogonal-view 3D images that were obtained from MSOT imaging recorded at varied time points after BX-BOH@BSA's injection (Fig. S17–S20, S22A and S22B, ESI†), it is apparent that for the sham group mice, there exist rather weak optoacoustic signals in the hepatic region in comparison with the HIRI model groups. As for the model groups in which the mice underwent ischemia for various time periods, the optoacoustic signals in the liver region become much stronger as the ischemia time is lengthened. Meanwhile, for the NAC group in which the model mice were treated with NAC, a much abated

optoacoustic signal exists in the liver. These MSOT imaging data corroborate the data from NIR-II fluorescent imaging experiments, and from these 3D MSOT images, HIRI's site and size can be observed more intuitively.

Moreover, the alanine transaminase (ALT) and aspartate aminotransferase (AST) levels in the mice's blood were measured by using ELISA kits, so as to evaluate the liver injury from the commonly-practiced perspective of the liver function evaluation.[25] As shown in Fig. S22C and D (ESI†), for the model groups (mice underwent ischemia for either 30 min or 60 min), the mice's ALT and AST levels in the blood are obviously higher than those for the sham group; this is indeed the case especially for the ''I/R: 60 min/24 h'' group, and the high blood ALT and AST levels confirm the liver injuries caused by the ischemia-reperfusion processes. Additionally, the liver tissues' histological evaluation (by H&E staining) was performed as well for the mice; as displayed in Fig. S22E (ESI†), the histological analysis data exhibit that the phenomena of hepatocyte vacuolation and necrosis are observable for the HIRI model mice with the extent becoming more severe for the mice undergoing longer ischemia time. In contrast, the sham group and the NAC group exhibit relatively normal morphology in the liver tissue sections.

In summary, we have developed a biomarker-responsive NIR-II fluorescent and optoacoustic nanoprobe BX-BOH@BSA for detecting and imaging HIRI. The probe compound can be activated by hepatic H_2O_2, thus generating evident optoacoustic and NIR-II fluorescent signals owing to the methylphenyl boronate group being removed and the subsequent transformation of the quaternized pyridyl into an uncharged pyridyl group. The nanoprobe BX-BOH@BSA may work as a utilizable tool for detecting HIRI, and the approach could provide useful ways of contriving other biomarker-responsive probes.

Conflicts of interest

There are no conflicts to declare.

Notes and references

1 Y. Zhai, H. Petrowsky, J. C. Hong, R. W. Busuttil and J. W. Kupiec-Weglinski, *Nat. Rev. Gastroenterol. Hepatol.*, 2013, **10**, 79–89.
2 B. L. Woolbright and H. Jaeschke, *Hepatology*, 2016, **63**, 1427–1429.
3 D. Xu, M. Xu, X. Kong and Q. Xia, *J. Hepatol.*, 2018, **69**, 746–758.
4 S. P. Monga, *Nat. Med.*, 2018, **24**, 6–7.
5 M. Cannistrà, M. Ruggiero, A. Zullo, G. Gallelli, S. Serafini, M. Maria, A. Naso, R. Grande, R. Serra and B. Nardo, *Int. J. Surg.*, 2016, **33**, S57–S70.
6 M. Peiseler and F. Tacke, *Hepatology*, 2021, **74**, 2888–2890.
7 Z. Qin, T. Ren, H. Zhou, X. Zhang, L. He, Z. Li, X. Zhang and L. Yuan, *Angew. Chem., Int. Ed.*, 2022, **61**, e202201541.
8 S. Zhu, R. Tian, A. L. Antaris, X. Chen and H. Dai, *Adv. Mater.*, 2019, **31**, 1900321.
9 L. Chen, J. Chen, Y. Fang, F. Zeng and S. Wu, *Chem. Commun.*, 2021, **57**, 7842–7845.
10 J. Chen, L. Chen, Y. Wu, Y. Fang, F. Zeng, S. Wu and Y. Zhao, *Nat. Commun.*, 2021, **12**, 6870.
11 W. Cheng, H. Chen, C. Liu, C. Ji, G. Ma and M. Yin, *View*, 2020, **1**, 20200055.
12 Q. Fu, R. Zhu, J. Song, H. Yang and X. Chen, *Adv. Mater.*, 2019, **31**, 1805875.
13 Y. Liu, L. Teng, B. Yin, H. Meng, X. Yin, S. Huan, G. Song and X. Zhang, *Chem. Rev.*, 2022, **122**, 6850–6918.
14 Y. Wu, F. Zeng, Y. Zhao and S. Wu, *Chem. Soc. Rev.*, 2021, **50**, 7924–7940.
15 J. Ouyang, L. Sun, F. Zeng and S. Wu, *Coord. Chem. Rev.*, 2022, **458**, 214438.
16 J. Ouyang, L. Sun, Z. Zeng, C. Zeng, F. Zeng and S. Wu, *Angew. Chem., Int. Ed.*, 2020, **59**, 10111–10121.
17 Z. Zhao, C. B. Swartchick and J. Chan, *Chem. Soc. Rev.*, 2022, **51**, 829–868.
18 L. Wu, Y. Ishigaki, W. Zeng, T. Harimoto, B. Yin, Y. Chen, S. Liao, Y. Liu, Y. Sun, X. Zhang, Y. Liu, Y. Liang, P. Sun, T. Suzuki, G. Song, Q. Fan and D. Ye, *Nat. Commun.*, 2021, **12**, 6145.
19 S. Lei, J. Zhang, N. T. Blum, M. Li, D. Zhang, W. Yin, F. Zhao, J. Lin and P. Huang, *Nat. Commun.*, 2022, **13**, 1298.
20 L. A. Kasatkina, C. Ma, M. E. Matlashov, T. Vu, M. Li, A. A. Kaberniuk, J. Yao and V. V. Verkhusha, *Nat. Commun.*, 2022, **13**, 2813.
21 X. Chen, Y. Wu, X. Ge, L. Lei, L. Niu, Q. Yang and L. Zheng, *Biosens. Bioelectron.*, 2022, **214**, 114510.
22 X. Lv, T. Han, Y. Wu, B. Zhang and W. Guo, *Chem. Commun.*, 2021, **57**, 9744–9747.
23 J. Liu, W. Zhang, C. Zhou, M. Li, X. Wang, W. Zhang, Z. Liu, L. Wu, T. D. James, P. Li and B. Tang, *J. Am. Chem. Soc.*, 2022, **144**, 13586–13599.
24 Y. Sun, L. Pu, L. Lu, X. Wang, F. Zhang and J. Rao, *World J. Gastroenterol.*, 2014, **20**, 15289–15298.
25 J. Nano, M. Ghanbari, W. Wang, P. S. Vries, K. Dhana, T. Muka, A. G. Uitterlinden, J. B. J. Meurs, A. Hofman, O. H. Franco, Q. Pan, S. D. Murad and A. Dehghan, *Gastroenterology*, 2017, **153**, 1096–1106.